PROCEEDINGS OF SCIENCE

Results from the fiducial volume analysis of the XMASS-RFB dark matter data

Atsushi Takeda for the XMASS collaboration[*†]
Kamioka Observatory, Institute for Cosmic Ray Research, the University of Tokyo, Higashi-Mozumi, Kamioka, Hida, Gify, 506-1205, Japan.
Kavli Institute for Physics and Mathematics for the Universe, the University of Tokyo, Kashiwa, Chiba 277-8582, Japan.
E-mail: takeda@km.icrr.u-tokyo.ac.jp

XMASS-I, the first phase of the XMASS project, is a direct detection dark matter experiment using a single-phase liquid xenon detector. The key idea to reduce the background at low energies in XMASS is to use liquid xenon itself as a shield. In this analysis the clean core of the liquid xenon volume is used as sensitive fiducial volume by eliminating the volume near the wall which sufferes from beta and gamma rays from the outside.

The XMASS-I detector has been refurbished for improvement of background reduction and data taking started on Nov. 2013, referred to as XMASS-RFB. In this talk, we will present the physics results for our direct dark matter search using the fiducial volume of the XMASS-RFB detector.

The 34th International Cosmic Ray Conference,
30 July- 6 August, 2015
The Hague, The Netherlands

[*]Speaker.
[†]A footnote may follow.

1. Introduction

XMASS is a multi-purpose detector using ultra pure liquid xenon aiming to detect dark matter, measure pp and ^{7}Be solar neutrinos, and observe neutrinoless double beta decay. The original idea is presented in [1]. The first phase of XMASS (XMASS-I) concentrates mainly on dark matter detection with more than 800 kg of liquid xenon in the active region.

The construction of the XMASS-I detector was completed in September 2010 at the Kamioka Observatory (2,700 m.w.e.) in Japan and commissioning runs were conducted from October 2010 to June 2012. Several physics results were obtained with the XMASS-I detector [2, 3, 4, 5]. From the commissioning run data, two main sources of background (BG) were identified. The first one is a radio-isotope (RI) contamination in the aluminum seal between the PMT entrance window and the metal body. The second one is RI on the inner surface of the detector, in particular on its oxygen free high conductivity (OFHC) copper. To eliminate events originating from above BG sources, the XMASS-I detector was refurbished in 2013, and data taking started on Nov. 2013 with the refurbished detector (XMASS-RFB). A detailed description of the XMASS-I detector is given in [6] and a detailed explanation for refurbishment work and the XMASS-RFB detector will be presented elsewhere in this conference.

Most of the observed events in the low energy region are coming from gamma and beta rays from RI contamination in PMTs and their support structure made of OFHC copper and RI attached to the surfaces of the detector. Their vertex positions are concentrated in the volume near the inner detector surface. To reduce this BG, a dedicated event reduction is applied based on vertex reconstruction and the clean core of the volume is used as fiducial volume. In this talk, we will present physics results using the fiducial volume of XMASS-RFB detector for direct dark matter search.

2. Vertex reconstruction

The vertex positions and energies of events were reconstructed using both information on the number of photo electrons (n PEs) and on their timing in each PMT. The PE based and the timing based reconstruction are calculated independently.

2.1 PE based reconstruction

The inner volume of the detector is based on grid points throughout the volume and on the surface for which the expected n PE distributions in each PMT are calculated in a Monte Carlo simulation (MC). The MC was developed based on Geant4 for the XMASS detector and simulates particle tracks, the scintillation process, the propagation of scintillation photons, the PMT response and our readout electronics [6]. The grid positions are on a Cartesian grid, on radial lines from the center of the detector, and on the inner surface of the detector. The calculated n PE distributions are normalized and treated as the probability density functions (PDFs) for each grid position. Using this PDF, the probability, $p_i(n)$, that the i-th PMT detects n PE is calculated. From the product of all $p_i(n_i)$, the likelihood function for each grid position $\mathbf{x}$ is calculated as:

$$L(\mathbf{x}) = \prod_{i=1}^{642} p_i(n_i), \tag{2.1}$$

where n_i represents nPE for the i-th PMT. The most likely position is obtained by maximizing L.

The performance of the vertex and energy reconstruction was evaluated using calibration data taken with several types of radioactive sources inserted in the detector. The upper panel of Fig. 1 shows the energy spectrum reconstructed using the ^{57}Co source at the detector center and the corresponding MC result. The lower panel of Fig. 1 shows the reconstructed vertices for various ^{57}Co source positions along the detector's vertical symmetry axis, z-axis. The distributions of the reconstructed energy and vertices for 122 keV gamma rays are reproduced well by our MC. We selected events inside the detector with a reconstructed PE based radius from s the center of detector (R(PE)) smaller than 20 cm. The signal acceptance in this selection were estimated using MC for several masses of WIMPs, and its value was 40% for events with reconstructed energy of 2-3 keVee by 100 GeV/c^2 WIMP.

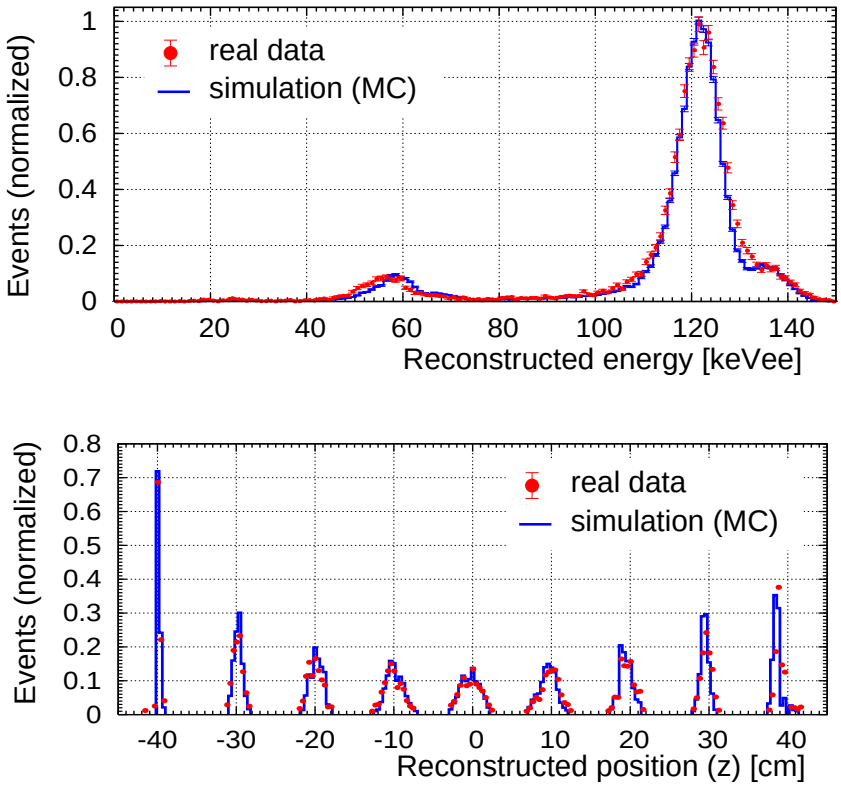

Figure 1: (Upper) Energy spectra reconstructed using ^{57}Co source at the detector center. (Lower) Vertex distributions reconstructed using the same source for data taken along the detector's vertical symmetry axis, the z-axis, at radii from the detector center -40, -30, ..., 30, 40 cm.

2.2 Timing based reconstruction

The timing distributions of each PMT from the grid points are also calculated using the MC, resulting in timing based PDFs $P(\tau)$. The product of all $P(\tau)$ for all hits in an event again becomes

the likelihood function of the assumed grid position $\mathbf{X}$ and event time T:

$$L(\mathbf{X},T) = \prod_{i=1}^{Nhits} P_i\left(t_i - \frac{|\mathbf{x}_i - \mathbf{X}|}{v_g} - T\right), \tag{2.2}$$

where $\mathbf{x}_i$ and t_i are position and hit time of i-th PMT, respectively, and v_g is the group velocity of scintillation light (110 mm/ns) in liquid xenon. The most likely position R(T) is obtained by maximizing L.

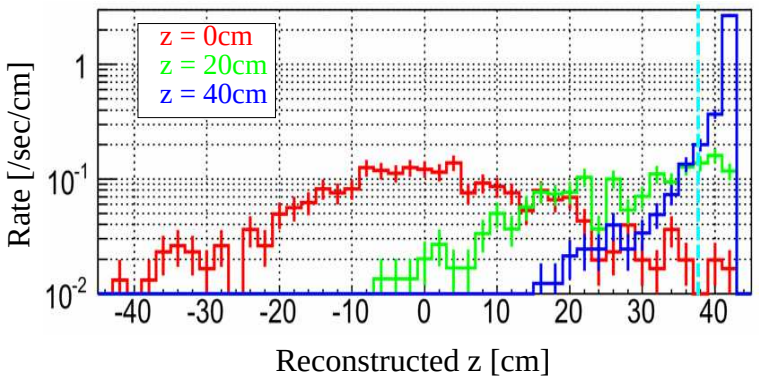

Figure 2: Vertex distributions from timing based reconstruction using ^{241}Am source for data taken along the detector's vertical symmetry axis, the z-axis, at radii from the detector center $0, 20, 40$ cm.

The performance of this vertex reconstruction was evaluated using the ^{241}Am source. Fig. 2 shows the reconstructed vertices for calibration data taken from source locations at various heights along the vertical detector axis. To remove events originating from the inner surface of the detector and maximize acceptance for events from inside the detector, events whose reconstructed R(T) is more than 38 cm were rejected. The signal acceptances after applying both the PE based fiducial cut ($\mathrm{R(PE)} < 20$ cm) and the timing based fiducial cut ($\mathrm{R(T)} < 38$ cm) was 19% for events with reconstructed energy of 2-3 keVee for our 100 GeV/c^2 WIMP MC.

3. Data reduction

The data used for this analysis were taken between Nov. 2013 and Jan. 2015 , and amount to a total live time of 292.66 days, excluding scheduled calibration data taking and detector maintenance work. After data quality checks rejecting data periods with unstable temperature and pressure, excessive PMT noise, unstable pedestal levels, or abnormal trigger rates, a dedicated data reduction procedure was applied. The dedicated data reduction proceeds in the following three steps:

(1) Standard reduction.

(2) Fiducial volume (radius) cuts.

(3) Decay time cut.

(1) To remove events caused by afterpulses, electronic noise, and Cherenkov events the standard reduction is applied to the raw data. Events that occur within 10 ms of the previous event are rejected to remove events caused by the tail of the energetic events. Events with a root mean square

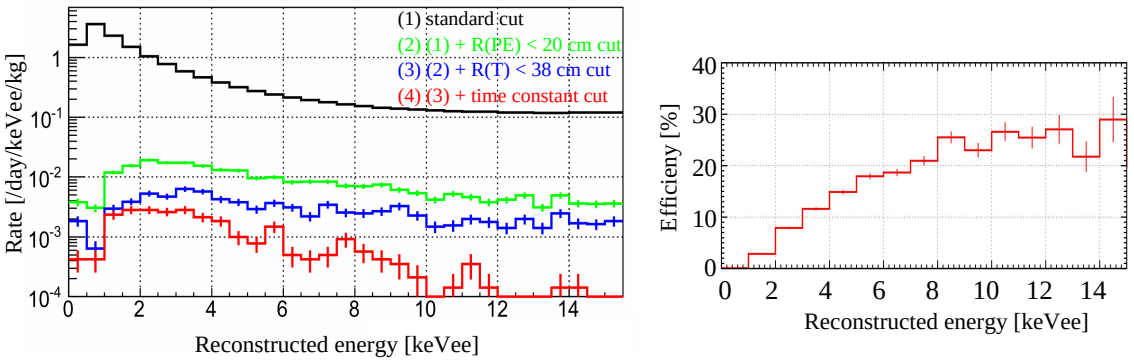

Figure 3: (Left) Energy spectrum after applying various data reduction steps. (Right) Signale efficiency after applying all cuts (corresponds to (4) in the left panel), obtained from our signal MC for a 100 GeV/c^2 WIMP.

of the hit timing larger than 100 ns are also rejected. In order to remove events which produce light predominantly through Cherenkov emission originating mainly from ^{40}K contamination in the PMT photocathodes events whose number of PMT hits in the first 20 ns divided by the total number of hits is larger than 0.6 are rejected if *n* PEs is less than 200.

(2) After applying the standard reduction, we reconstruct the vertex positions of each event using both the PE and timing based reconstruction. For reliable and good signal efficiency, enough *n* PEs and hits are needed for vertex reconstruction. We set an energy threshold of 2 keVee for vertex reconstruction. Events with $\mathrm{R(PE)} < 20$ cm and $\mathrm{R(T)} < 38$ cm are kept.

(3) To select nuclear recoils, the scintillation decay time of each event was extracted from wave form information of all PMTs. The timing constant for nuclear recoil events as a function of reconstructed energy was taken from neutron calibration data and implemented in our MC. The cut on the timing constant was chosen to give a signal efficiency of 50%. s

Fig. 3 shows the obtained energy spectrum from 292.66 live days of data after applying successive data reductions and the signal efficiency applying all cuts for 100 GeV/c^2 WIMP calculated from our MC. The event rate with reconstructed energy of 2-3 keVee after all cuts was 2.7 ± 0.3 counts/day/keVee/kg and the signal efficiency for 100 GeV/c^2 WIMP was 9% for this same energy range.

4. Results and discussion

Fig. 4 shows the obtained energy spectrum from 292.66 live days of data applying all cuts and the expected signal for 100 GeV/c^2 WIMP calculated by our MC. WIMPs are assumed to be distributed in an isothermal halo with $v_0 = 220$ km/s , an escape velocity of $v_{esc} = 650$ km/s, and to have 0.3 GeV/cm^3 average density. For conversion from nuclear recoil equivalent energy to electron equivalent energy (keVee), the scintillation efficiency, $\mathscr{L}_{\mathrm{eff}}$, for nuclear recoils relative to that of 122 keV gammas at zero electric field was taken from [7]. The upper limit of cross section was obtained requiring that the expected event rate with statistic and all systematic errors does not exceed the observed rate in any energy bin above the 2 keVee energy threshold. The most

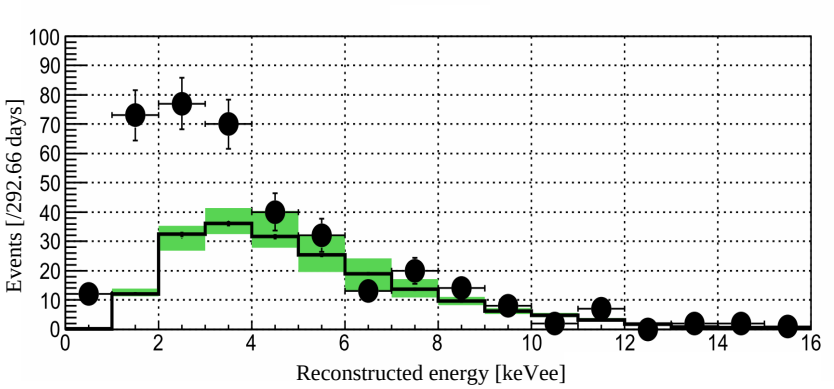

Figure 4: Obtained energy spectrum after applying all cuts (black dots), and expected 100 GeV/c^2 WIMP signal (black histogram) with all the systematic errors (green hatched) for a spin-independent cross section of 1.60×10^{-43} cm^3.

constraining energy bin for setting this limit was the 6-7 keVee bin. The 90% C.L. upper limit for 100 GeV/c^2 WIMP was 1.60×10^{-43} cm^3 with statistic and systematic errors.

The green band in fig. 4 reflects all our systematic uncertainties. The systematic uncertainty on signal efficiency was estimated from comparison between data and MC by using calibration data from ^{241}Am for the fiducial volume cuts and from ^{252}Cf for the decay time cut. The values for the 6-7 keVee bin were -1.5+2.0% and -20+10% for the fiducial volume and decay time cuts, respectively. The systematic uncertainty coming from the uncertainty for scintillation decay time constant of nuclear recoils implemented in our MC (25+1-2 ns) is -10.2+17.1%. The systematic uncertainty for our energy scale was coming mainly from variation of the absorption length for scintillation light in liquid xenon during data taking. From the regularly scheduled calibration data taken with ^{57}Co located inside the detector and ^{60}Co irradiating from the outside of the detector, the absorption length of each period was calculated by MC and the systematic uncertainty was evaluated. It was -11.8+13.7% for the 6-7 keVee energy bin. The uncertainty for $\mathscr{L}_{\rm eff}$ was -30+28%.

According to our MC, the remaining events in fig. 4 are mainly coming from RI contamination on our OFHC copper support structure. We do not subtract this BG when calculating our limit. After completion of our BG study, a more stringent limit will be derived after subtracting BG.

5. Conclusion

A fiducial volume based dark matter search was performed using 292.66 live days of data from the XMASS-RFB detector. After a data reduction mainly based on fiducial volume cuts, upper limits for several WIMP masses were obtained. Our 90% C.L. upper limit for a 100 GeV/c^2 WIMP is 1.60×10^{-43} cm^3 including statistic and systematic errors.

References

[1] Y. Suzuki, arXiv:hep-ph/0008296.

[2] K. Abe *et al.* (the XMASS collaboration), Phys. Lett. **B 719** (2013) p. 78-82.

[3] K. Abe *et al.* (the XMASS collaboration), Phys. Lett. **B 724** (2013) p. 46-50.

[4] H. Uchida *et al.* (the XMASS collaboration), PTEP **063C01** (2014).

[5] K. Abe *et al.* (the XMASS collaboration), Phys. Rev. Lett. **113** (2014) 121301.

[6] K. Abe *et al.* (the XMASS collaboration), Nucl. Instr. and Meth. **A 716** (2013) p. 78-85.

[7] E. April *et al.*, Phys. Rev. Lett. **107** (2011) 131302.